Pathway-dependent fate of permafrost region carbon

Environmental Research Letters

LETTER

Pathway-dependent fate of permafrost region carbon

Thomas Kleinen and Victor Brovkin

Max Planck Institute for Meteorology, Bundesstr. 53, D-20146 Hamburg, Germany

E-mail: thomas.kleinen@mpimet.mpg.de

OPEN ACCESS

RECEIVED
27 March 2018

REVISED
13 July 2018

ACCEPTED FOR PUBLICATION
6 August 2018

PUBLISHED
20 August 2018

Keywords: permafrost carbon, climate change, land surface modelling, carbon balance, CO_2 fertilisation

Supplementary material for this article is available online

Abstract

Permafrost soils in the high northern latitudes contain a substantial amount of carbon which is not decomposed due to frozen conditions. Climate change will lead to a thawing of at least part of the permafrost, implying that the stored carbon will become accessible to decomposition and be released to the atmosphere. We use a land surface model to quantify the amount of carbon released up until 2300 and determine the net carbon balance of the northern hemisphere permafrost region under climate warming following the RCP scenarios 2.6, 4.5, and 8.5. Here we show for the first time that the net carbon balance of the permafrost region is not just strongly dependent on the overall warming, but also on the CO_2 concentration pathway. As a result moderate warming scenarios may counter-intuitively lead to lower net carbon emissions from the permafrost region than low warming scenarios.

1. Introduction

Permafrost soils in the high northern latitudes contain substantial amounts of carbon (C) which are not accessible to decomposition due to frozen conditions. Current estimates put the C content of soils in the northern circumpolar region in the order of 1300 PgC, with a substantial fraction of this carbon stored in perennially frozen ground (Hugelius *et al* 2014). However, climate change will lead to thaw of at least part of the perennially frozen permafrost (Koven *et al* 2013), implying that the stored carbon will become accessible to decomposition and potentially be released to the atmosphere.

The potential carbon release from northern hemisphere (NH) permafrost thaw has been investigated in a number of modelling studies (McGuire *et al* 2010, 2018, Koven *et al* 2011, 2015, Schaefer *et al* 2011, Schneider von Deimling *et al* 2012, 2015, Burke *et al* 2017). These, as well as review studies (McGuire *et al* 2010, Schaefer *et al* 2014, Schuur *et al* 2015), point to critical factors to be considered. McGuire *et al* (2018) show that large effects of permafrost thaw are to be expected in the 22nd and 23rd centuries, making studies that limit the time horizon to the 21st century of limited value. Model studies that use model-derived carbon stocks as initial conditions increase uncertainty about permafrost carbon stocks and emissions, as the modelled initial stocks may differ widely from observations (see Schaefer *et al* 2014 for an overview). Furthermore, large changes in vegetation productivity are to be expected under future climate conditions, pointing to a need to include these, in addition to C release from thawing permafrost soils, in a full C balance of the NH permafrost region (McGuire *et al* 2010, 2018, Koven *et al* 2011).

We therefore aim to improve on the existing studies. We use a land surface model to quantify the amount of carbon released until 2300 and determine the net carbon balance of the NH permafrost region under climate warming following the representative concentration pathway (RCP) scenarios 2.6, 4.5, and 8.5 (Meinshausen *et al* 2011). We initialise the the frozen carbon stocks from an observation-based data set (Hugelius *et al* 2013), ensuring that initial conditions are close to observations, similar to Jafarov and Schaefer (2016), but different from Koven *et al* (2015) in that we use a full land surface model to estimate fluxes. We finally determine the cumulative net C flux to assess the effect of permafrost region C cycle changes on climate.

2. Materials and methods

2.1. JSBACH

We use the Max Planck Institute Earth System Model (MPI-ESM) (Giorgetta *et al* 2013) land surface scheme JSBACH (Brovkin *et al* 2013, Reick *et al* 2013, Schneck *et al* 2013) in resolution T63 (1.875° × 1.875°) to investigate the changes to the NH permafrost region net carbon balance under global warming. In comparison to the CMIP5 version published previously, we have extended the model with a multilayer hydrology scheme (Hagemann and Stacke 2015), using 11 soil layers in the experiments described here, with increasing thicknesses from 6.5 cm at the surface to 23.2 m at the bottom, coming to a total soil column depth of 52.14 m. We have also added a representation of permafrost physical processes (Ekici *et al* 2014), including soil insulation by a surface organic layer, as well as the improved soil carbon model YASSO (Tuomi *et al* 2008, 2009, 2011, Goll *et al* 2015) for soil organic matter (SOM) decomposition. Vegetation disturbances from windbreak and fire are included in the model, with windbreak dependent on the wind velocity and fire dependent on litter amount and humidity. In addition herbivory is considered as a fixed fraction of net primary production.

As implemented in JSBACH (Goll *et al* 2015), YASSO represents SOM as carbon solubility fractions. It distinguishes litter in acid soluble (A), water soluble (W), ethanol soluble (E) and non-soluble (N) fractions, with the pools replicated for above- and belowground. In addition to the litter pools, a humus pool contains carbon that decomposes on long timescales. These pools are replicated for green and woody litter on each vegetation tile. A simplified schematic is shown in the SI, figure S1(a) available online at stacks.iop.org/ERL/13/094001/mmedia. We have extended the YASSO model to represent permafrost carbon stocks. We estimate the thickness of the active layer (AL), the part of the soil column that thaws during the summer season, from the modelled 2 year mean thaw depth, inspired by the definition of permafrost as ground that remains frozen for at least two consecutive years. Carbon cycling in the AL is represented by the YASSO model, while frozen carbon stocks below the AL are prescribed from the Northern Circumpolar Soil Carbon Database (NCSCD), version 2 (Hugelius *et al* 2013), thereby insuring that the carbon stocks are in line with observations. As the AL thickness increases under climate warming, we transfer carbon from the prescribed frozen carbon stocks into the AL pools described by the YASSO model, as shown schematically in SI figure S1b. The carbon amount transferred is proportional to the change in AL thickness, and the transferred carbon is allocated to the different YASSO carbon pools according to pool proportions in preindustrial (PI) climate. We therefore assume that conditions in preindustrial climate are representative for the conditions under which the permafrost C stocks formed.

2.2. Permafrost C initialisation

Hugelius *et al* (2014) estimate a total C stock of ~1300 PgC for the northern circumpolar region, with 1035 ± 150 PgC in the depth range to 3 m depth. The NCSCD (Hugelius *et al* 2013) contains estimates of the soil carbon stock in the northern circumpolar region in four depth intervals, 0–30 cm, 0–100 cm, 100–200 cm, and 200–300 cm. We convert the second depth interval to 30–100 cm by subtracting the C stock for 0–30 cm from the one for 0–100 cm and perform a conservative remapping of the carbon stocks from the native 0.5° grid to the T63 (~1.875°) resolution of JSBACH. After remapping, the NCSCD estimates a total C stock of 1151 PgC to 3 m depth in the northern circumpolar region. Of this total stock, 22 PgC are located in areas covered by the JSBACH glacier mask, mostly on the margins of the Greenland Ice Sheet, and 52 PgC lie outside the land-sea mask employed by JSBACH, mostly along the northern coasts of Canada and Siberia. A further 127 PgC are located in regions, where JSBACH does not model permafrost in preindustrial climate, despite the fact that the permafrost region is represented reasonably well in JSBACH, with a total area with AL depths less than 3 m in preindustrial climate of 20×10^6 km^2, similar to area estimates from the Brown *et al* (2002) map. Overall this leaves a total carbon stock of 949 PgC in the permafrost area modelled by JSBACH.

For model initialisation, the AL thickness is diagnosed by determining the 2 year mean thaw depth for the preindustrial state (SI figure S2). The carbon stock in the NCSCD below the diagnosed maximum AL thickness is used to initialise frozen C pools in the model at the start of the historical experiment. Using the depth information in the NCSCD and the AL thickness modelled in JSBACH for preindustrial climate, 258 PgC are located in the AL, while 691 PgC are at depths below the modelled AL thickness and are prescribed as initial conditions for the frozen permafrost carbon.

Comparing the distribution of carbon in the AL for the start of our experiments in 1850 (SI figure S3) JSBACH/YASSO underestimates AL carbon by 95 PgC in total. However, the spatial pattern shows that the largest underestimates are in areas of organic soils (SI figure S7(a)), which are not represented explicitly in JSBACH. In addition the NCSCD was compiled from recent measurements and therefore is not representative of preindustrial conditions, but rather of present-day conditions. Performing the comparison for the end of the historical experiments reduces the bias slightly (not shown), though the spatial pattern remains similar.

Hugelius *et al* (2014) estimate an uncertainty range for the total NCSCD carbon stock of 1035 ± 150 PgC,

an uncertainty of ±14.5%. We use their uncertainty estimate for the total permafrost C stock to derive an uncertainty range for the model results, as the uncertainty in frozen C stock translates directly into an uncertainty of possible soil carbon gain through thawing of permafrost.

2.3. Experiments

We perform a set of experiments with JSBACH, driven by climate forcings from CMIP5 experiments performed with MPI-ESM (Giorgetta *et al* 2013). These climate forcings were available for the extended period until 2300 and produced using an earlier version of the same model, allowing a relatively consistent setup of the experiments. We use climate forcings for the historical period 1850–2005, followed by three experiments to 2300 using the scenarios RCP 2.6, RCP 4.5, and RCP 8.5 (Meinshausen *et al* 2011). We use the scenarios extended to 2300, with CO_2 stabilised at 542.9 ppm in RCP 4.5 and at 1 961.58 ppm in RCP 8.5, while CO_2 peaks at 442.76 ppm in 2050 for RCP 2.6, thereafter decreasing to 327.21 ppm. For completeness land use changes are included in the scenario experiments, though their impact in the permafrost region is negligible due to the very small areas affected. The model is run in a global configuration, though only results for the permafrost region are shown, i.e. the region with AL thicknesses smaller than 3 m (SI figure S2). We consider paired experiments with and without the consideration of permafrost C to determine the role of thawing permafrost carbon.

For the historical period, as well as scenarios RCPs 2.6 and 4.5, we also perform two additional experiments each to differentiate between the effects of changes in CO_2 and climate. In one of these we keep CO_2 fixed at the PI level of 285 ppm but impose the climate forcings from the scenario experiment, while we vary CO_2 according to the scenario but impose a climate forcing from the PI control climate in the second.

Prior to the start of the experiments, we performed a model initialisation under preindustrial conditions, forced by the climate forcings from the PI control experiment with MPI-ESM. The model carbon cycle initialisation consisted of a 300 year spinup of the model physics, followed by a 5000 year spinup of the carbon cycle to a state in equilibrium with climate. Combining the physics and carbon states, the model was integrated for a further 400 years to ensure consistency. In the spinup experiments, permafrost C pools were not considered, these were only initialised at the start of the historical experiment.

2.4. Permafrost carbon feedback

To determine the feedback of permafrost region C cycle changes on climate, one would ideally perform experiments similar to the ones we have made with a full ESM, including an oceanic carbon cycle. As this was not possible for the present study, we determine the permafrost carbon feedback in a simplified way. We use the airborne fraction of emitted CO_2 (f_A) for the three scenarios from Jones *et al* (2013) to convert the difference in the cumulative net C flux between the permafrost and the non-permafrost experiments ΔC_{net} into a change in atmospheric CO_2 concentration ΔCO_2^P using $\Delta CO_2^P = \Delta C_{net} \times f_A \times 2.12$ GtC ppm^{-1}. Using ΔCO_2 and a climate sensitivity α of 3 K, we determine the change in global mean temperature due to the changes in the permafrost region carbon balance ΔT^P from $\Delta T^P = \alpha \times (\ln((CO_2 + \Delta CO_2^P)/280) - \ln(CO_2/280))$. Using ΔT and ΔCO_2, the change in global mean temperature (from the CMIP5 experiments without considering permafrost) and the change in atmospheric CO_2 concentration (from the RCP scenario), we determine the ratio $\Delta T^P/\Delta T$ as the temperature gain and the ratio $\Delta CO_2^P/\Delta CO_2$ as the CO_2 gain due to the permafrost carbon feedback.

3. Results

3.1. Permafrost carbon thaw

Climatic changes in the historical and scenario experiments, especially increasing temperatures, lead to an increase in the depth of the AL, the soil layer thawing during the summer season. Thereby carbon contained in soil layers that were perennially frozen under preindustrial conditions becomes available to active carbon cycling. The initial frozen carbon stock of 691 ± 100 PgC decreases during the historical period to 630 PgC in 2005 (figure 1(a)), with further changes depending on the scenario assumed (table 1). The smallest decline occurs in RCP 2.6, where stocks are reduced by 135 ± 20 PgC in 2075, with only small changes afterwards, while the entire stock of frozen C becomes available for decomposition in RCP 8.5, with 65% of the carbon thawed by 2100 and the remainder thawing during the 22nd century. Finally, RCP 4.5 leads to a reduction in frozen C to 325 ± 47 PgC by 2300, leaving nearly half the PI frozen carbon stock in frozen state. As permafrost carbon thaws, C stocks in the AL increase (figure 1(b)) leading to enhanced heterotrophic respiration (R_h) in comparison to experiments without permafrost C, as more carbon is available for decomposition (SI figure S6).

3.2. Net carbon flux

For an evaluation of the impacts of permafrost thaw on climate, however, we need to assess changes in the net carbon flux from the land surface. The net C flux is comprised of carbon uptake through net primary productivity (NPP) and carbon release through heterotrophic respiration (R_h), as well as further carbon fluxes from land use change (C_{LUC}), fire (D_f), windthrow (D_w) and herbivory (D_h). These further fluxes are very small in comparison to NPP and R_h, and they generally show a release of carbon. As initial analysis showed no strong

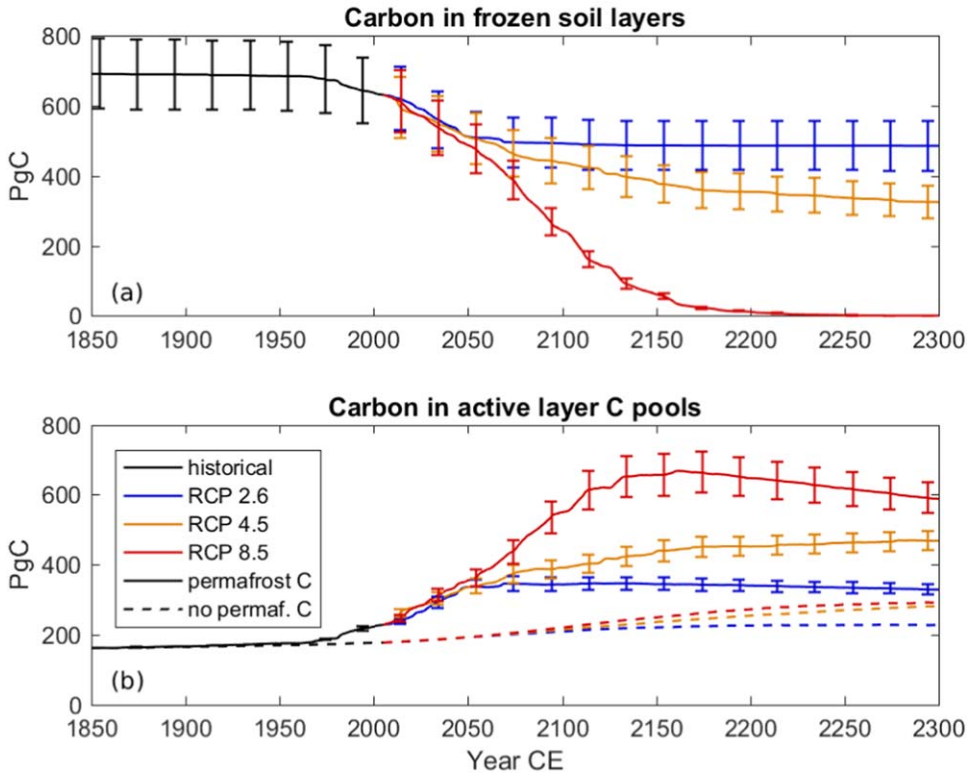

Figure 1. Simulated carbon stocks in frozen (a) and active layers (b) for the NH permafrost region (as shown in SI figure S2). Error bars show the uncertainty derived from the permafrost C uncertainty range by Hugelius *et al* (2014).

Table 1. Carbon fluxes and pools sizes for 1850, 2005, 2100, and 2300, with 2050 also given for RCP 2.6. Values in parentheses refer to experiments without permafrost C.

Scenario	NPP (PgC/a)	R_h (PgC/a)	net C (PgC/a)	Cum. net C (PgC)	Frozen C (PgC)	Act. lay. C (PgC)
			1850			
Hist	3.5	3.5	0.0	0.0	691 (0)	162 (162)
			2005			
Hist	5.1	5.1 (4.8)	0.0 (0.3)	7.6 (17.6)	630 (0)	229 (178)
			2050			
2.6	6.8	7.0 (6.2)	−0.2 (0.6)	8.4 (44.5)	514 (0)	333 (192)
			2100			
2.6	6.9	7.0 (6.5)	−0.1 (0.4)	5.6 (69.0)	492 (0)	344 (209)
4.5	8.3	8.2 (7.5)	0.1 (0.8)	7.2 (83.0)	437 (0)	391 (215)
8.5	11.3	11.8 (10.0)	−0.5 (1.3)	−11.5 (105)	243 (0)	550 (220)
			2300			
2.6	6.0	6.1 (6.0)	−0.1 (0.0)	−23.6 (79.2)	485 (0)	329 (228)
4.5	10.1	10.2 (9.8)	−0.1 (0.3)	9.2 (185)	326 (0)	469 (281)
8.5	19.5	19.9 (19.2)	−0.4 (0.3)	−104 (285)	0 (0)	590 (292)

impact of these fluxes, we include them in the R_h flux for the following discussion, noting that their importance may be more pronounced on local to regional scales (Genet *et al* 2018). The full net C flux therefore is defined as $C_{net} = \mathrm{NPP} - (R_h + D_f + D_w + D_h + C_{LUC})$, and in the following we discuss the combined C release flux $R_h + D_f + D_w + D_h + C_{LUC}$, which we imprecisely call R_h as this is the major component.

As atmospheric CO_2 and temperature rise, NPP (with positive NPP indicating a carbon uptake by vegetation) in the northern high latitudes increases due to two factors: warmer climatic conditions lead to longer

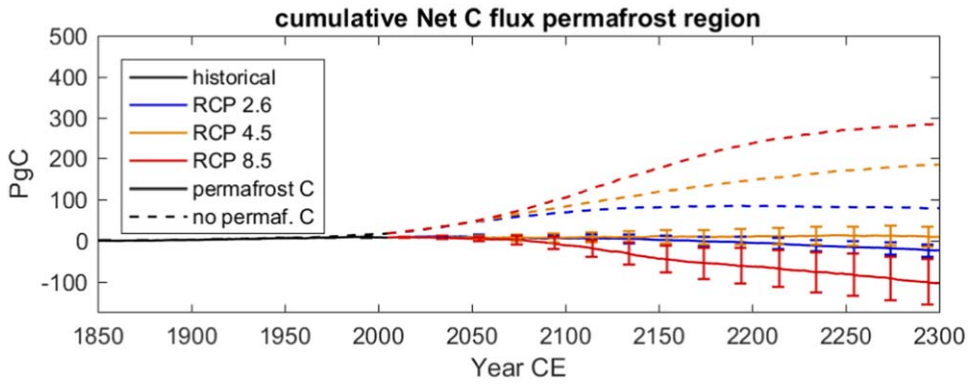

Figure 2. Cumulative net carbon uptake of the permafrost region. Solid lines show experiments with frozen permafrost C considered, dashed lines experiments without permafrost C. Error bars show the uncertainty derived from the permafrost C uncertainty range by Hugelius *et al* (2014).

Table 2. Permafrost carbon feedback gain for atmospheric CO_2 and global mean temperature, in %. The feedback strength is calculated relative to the preindustrial state.

Scenario	C loss (PgC)	ΔCO_2^P (ppm)	ΔT^P (K)	CO_2 gain (%)	T gain (%)
			2100		
2.6	63 ± 9	9 ± 1	0.06 ± 0.01	6.3 ± 0.9	3.7 ± 0.5
4.5	76 ± 11	14 ± 2	0.08 ± 0.01	5.6 ± 0.8	3.0 ± 0.4
8.5	116 ± 17	36 ± 4	0.11 ± 0.02	5.4 ± 0.8	2.2 ± 0.3
			2300		
2.6	103 ± 15	15 ± 2	0.12 ± 0.03	18.0 ± 2.6	9.1 ± 1.3
4.5	175 ± 25	33 ± 5	0.18 ± 0.02	12.6 ± 1.8	5.6 ± 0.8
8.5	389 ± 56	119 ± 17	0.18 ± 0.02	7.1 ± 1.0	1.7 ± 0.2

growing seasons, enhancing plant growth, and more CO_2 leads to higher carbon assimilation in photosynthesis, as C assimilation is dependent on the leaf surface CO_2 concentration in the Farquhar *et al* (1980) photosynthesis model employed in JSBACH. The impact of climate and CO_2 changes on NPP is of similar magnitude, with a substantial synergy between the two factors (supplementary information and SI figure S9). As a result, we obtain an increase in NPP over the historical period, as well as in all scenario experiments (table 1 and SI figure S6(a)).

R_h (with positive R_h indicating a release of carbon from the land surface) also grows in all experiments, due to temperature-related increases in respiration rate, as well as AL carbon accumulation (table 1 and SI figure S6(b)). If permafrost C is considered, the latter factor is strongly enhanced due to the transfer of carbon from formerly frozen soil layers into the AL. Therefore the increase in R_h is substantially stronger if permafrost C is considered. Details of carbon pool and flux changes are given in table 1, as well as in the supplementary information. Without considering permafrost C the climatically relevant net carbon flux NPP $-$ R_h is generally positive, indicating a net uptake of carbon by the land surface. When considering permafrost C, however, the net C flux is decreased markedly, turning negative in most cases (table 1).

There is a well-established relationship between cumulative carbon emissions and global temperature change (Matthews *et al* 2009, Zickfeld *et al* 2012, Gillett *et al* 2013). Consequently we focus on the cumulative net C flux from the NH permafrost region in order to assess the climate feedback of NH permafrost carbon thaw (figure 2). For RCP 2.6 with permafrost C the cumulative net flux in 2300 is −24 PgC (79 PgC without permafrost C), while it is 9.6 PgC (185 PgC without permafrost C) for RCP 4.5, and −104 PgC (285 PgC without permafrost C) for RCP 8.5. Accounting for permafrost carbon thus reduces the cumulative net C uptake to 2300 by 103 ± 14.9 PgC, 175 ± 25.4 PgC, or 389 ± 56.4 PgC, respectively, for RCPs 2.6, 4.5, and 8.5.

With these results for the changes in the cumulative net carbon balance, we can estimate the permafrost carbon feedback gain from the difference in the cumulative net C flux ('C loss' in table 2). The method described in section 2.4 allows us to estimate the feedback of permafrost region C cycle changes on climate, determining the additional CO_2 in the atmosphere, as well as the additional warming. The CO_2 and

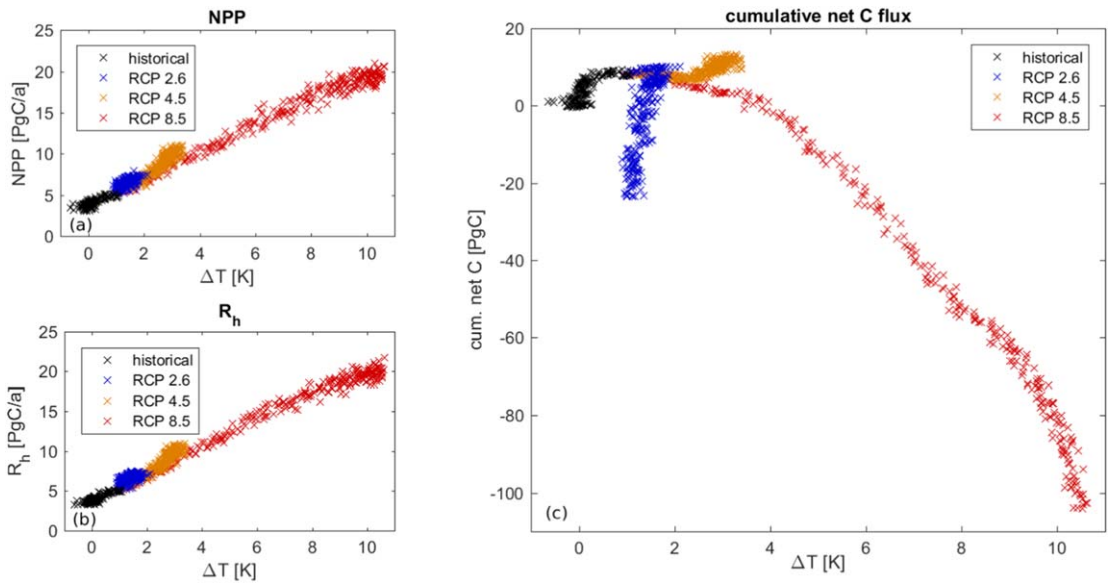

Figure 3. Relation of NH permafrost region NPP (a), R_h (b) and cumulative net C flux (c) to global mean temperature change in experiments with permafrost carbon considered.

temperature gains for 2300 are largest for RCP 2.6, with a CO_2 gain of 18% and a temperature gain of 9%, while they are substantially smaller (7% for CO_2 and 2% for temperature) for RCP 8.5. The impact of permafrost region carbon cycle changes therefore is much more relevant to climate change under the low-emission RCP 2.6 than under the higher emission scenarios.

3.3. Pathway-dependence

Concentrating on the case with permafrost carbon, we consider how the net carbon balance changes with global warming. Here NPP and R_h to first order change linearly with global mean temperature change (figures 3(a) and (b)), implying that changes in these fluxes are independent of the exact greenhouse gas trajectory and mainly dependent on warming. Investigating the cumulative net flux, however, no such linear relationship can be found (figure 3(c)). Instead, the different scenarios clearly fall on different trajectories, showing a dependence of the cumulative net C flux not just on the global mean temperature change, but also on the pathway this was arrived at. This pathway-dependence is due to a combination of factors. First, the net flux, being the difference between NPP and R_h, is substantially smaller than the component fluxes, emphasising changes in the component fluxes. Second, the change in NPP is not just dependent on temperature change, but through CO_2-fertilisation also on the atmospheric CO_2 concentration. As a result NPP keeps increasing until the end of the experiments in RCPs 4.5 and 8.5, while it reaches a maximum in 2113 and decreases subsequently in RCP 2.6. Third, warming in RCPs 2.6 and 4.5 is substantially smaller than in RCP 8.5, keeping a substantial fraction of the PI permafrost C in frozen state, thereby limiting the increase in R_h. The combination of these factors leads to the separation of trajectories observed in our experiments (figure 3(c)).

4. Conclusions

We have shown that the mobilisation and partial respiration of thawed permafrost C significantly reduces the net carbon fluxes into the permafrost region. The magnitude of the reduction in net carbon flux is smallest in the RCP 2.6 scenario and largest in the RCP 8.5 scenario. Taking into account the extent of anthropogenic perturbations to the climate system, however, this ranking is reversed. RCP 2.6 assumes anthropogenic emissions of −0.42 PgC/a, i.e. an anthropogenic removal of carbon, for the year 2100. If permafrost C is considered, the net C flux into the permafrost region is decreased by 0.4 PgC/a, implying that the negative emissions would need to be doubled in order to reach the climate target. This ranking is also reflected in the substantially larger permafrost carbon feedback gains in RCP 2.6 than in RCPs 4.5 and 8.5.

Our results also show the importance of the time horizon considered. While permafrost thaw has limited carbon cycle implications during the 21st century, the relevance becomes substantially larger, if longer time horizons are considered, as part of the permafrost C remains frozen in 2100 even in the high warming RCP 8.5 scenario.

Finally, our results demonstrate that the trajectory of the climate system to a final climate state has consequences for the net carbon emissions from the permafrost region. The NH permafrost region becomes a net source of carbon in both the strong warming scenario RCP 8.5, and in the climate stabilisation

scenario RCP 2.6. With the intermediate scenario RCP 4.5, however, the NH permafrost region remains a (small) net sink of carbon, despite a stronger warming than in RCP 2.6. This is mainly due to the enhanced carbon uptake through CO_2-fertilisation under the higher CO_2 concentrations and longer growing seasons of RCP 4.5. Thus the fate of the permafrost region carbon is not only dependent on the overall warming, but also on the climate trajectory, it is pathway-dependent.

Acknowledgments

The research leading to these results was made possible by the CarboPerm project funded by the German Ministry of Education and Research (BMBF Grant No. 03G0836C). We thank Christian Beer, Christian Knoblauch, Thomas Schneider von Deimling, Gustaf Hugelius and the Permafrost Carbon network for many stimulating discussions, as well as Tom Riddick for comments on an earlier draft of this manuscript. We also thank two anonymous reviewers who provided very constructive comments.

Data availability

Primary data and scripts used in the analysis and other supplementary information that may be useful in reproducing the authors work are archived by the Max Planck Institute for Meteorology and can be obtained by contacting the first author or publications@mpimet.mpg.de.

ORCID iDs

Thomas Kleinen https://orcid.org/0000-0001-9550-5164
Victor Brovkin https://orcid.org/0000-0001-6420-3198

References

Brovkin V, Boysen L, Raddatz T, Gayler V, Loew A and Claussen M 2013 Evaluation of vegetation cover and land-surface albedo in MPI-ESM CMIP5 simulations *J. Adv. Model. Earth Syst.* **5** 48–57

Brown J, Ferrians O, Heginbottom J A and Melnikov E 2002 *Circum-Arctic Map of Permafrost and Ground-ice Conditions, Version 2* (Boulder, Colorado: NSIDC: National Snow and Ice Data Center)

Burke E J, Ekici A, Huang Y, Chadburn S E, Huntingford C, Ciais P, Friedlingstein P, Peng S and Krinner G 2017 Quantifying uncertainties of permafrost carbon-climate feedbacks *Biogeosciences* **14** 3051–66

Ekici A, Beer C, Hagemann S, Boike J, Langer M and Hauck C 2014 Simulating high-latitude permafrost regions by the JSBACH terrestrial ecosystem model *Geosci. Model Dev.* **7** 631–47

Farquhar G D, von Caemmerer S and Berry J A 1980 A biochemical model of photosynthetic CO_2 assimilation in leaves of C3 species *Planta* **149** 78–90

Genet H *et al* 2018 The role of driving factors in historical and projected carbon dynamics of upland ecosystems in Alaska *Ecol. Appl.* **28** 5–27

Gillett N P, Arora V K, Matthews D and Allen M R 2013 Constraining the ratio of global warming to cumulative CO_2 emissions using CMIP5 simulations *J. Clim.* **26** 6844–58

Giorgetta M A *et al* 2013 Climate and carbon cycle changes from 1850 to 2100 in MPI-ESM simulations for the Coupled Model Intercomparison Project phase 5 *J. Adv. Model. Earth Syst.* **5** 572–97

Goll D S, Brovkin V, Liski J, Raddatz T, Thum T and Todd-Brown K E O 2015 Strong dependence of CO_2 emissions from anthropogenic land cover change on initial land cover and soil carbon parametrization *Glob. Biogeochem. Cycles* **29** 1511–23

Hagemann S and Stacke T 2015 Impact of the soil hydrology scheme on simulated soil moisture memory *Clim. Dyn.* **44** 1731–50

Hugelius G *et al* 2013 A new data set for estimating organic carbon storage to 3 m depth in soils of the northern circumpolar permafrost region *Earth Syst. Sci. Data* **5** 393–402

Hugelius G *et al* 2014 Estimated stocks of circumpolar permafrost carbon with quantified uncertainty ranges and identified data gaps *Biogeosciences* **11** 6573–93

Jafarov E and Schaefer K 2016 The importance of a surface organic layer in simulating permafrost thermal and carbon dynamics *Cryosphere* **10** 465–75

Jones C *et al* 2013 Twenty-first-century compatible CO_2 emissions and airborne fraction simulated by CMIP5 earth system models under four representative concentration pathways *J. Clim.* **26** 4398–413

Koven C D, Ringeval B, Friedlingstein P, Ciais P, Cadule P, Khvorostyanov D, Krinner G and Tarnocai C 2011 Permafrost carbon-climate feedbacks accelerate global warming *Proc. Natl Acad. Sci.* **108** 14769–74

Koven C D, Riley W J and Stern A 2013 Analysis of permafrost thermal dynamics and response to climate change in the CMIP5 Earth System Models *J. Clim.* **26** 1877–900

Koven C D *et al* 2015 A simplified, data-constrained approach to estimate the permafrost carbon–climate feedback *Phil. Trans. R. Soc.* A **373** 1–23

Matthews H D, Gillett N P, Stott P A and Zickfeld K 2009 The proportionality of global warming to cumulative carbon emissions *Nature* **459** 829

McGuire A D, Macdonald R W, Schuur E A, Harden J W, Kuhry P, Hayes D J, Christensen T R and Heimann M 2010 The carbon budget of the northern cryosphere region *Curr. Opin. Environ. Sustainability* **2** 231–6

McGuire A D *et al* 2018 Dependence of the evolution of carbon dynamics in the northern permafrost region on the trajectory of climate change *Proc. Natl Acad. Sci.* **115** 3882–7

Meinshausen M *et al* 2011 The RCP greenhouse gas concentrations and their extensions from 1765 to 2300 *Clim. Change* **109** 213

Reick C H, Raddatz T, Brovkin V and Gayler V 2013 Representation of natural and anthropogenic land cover change in MPI-ESM *J. Adv. Model. Earth Syst.* **5** 459–82

Schaefer K, Lantuit H, Romanovsky V E, Schuur E A G and Witt R 2014 The impact of the permafrost carbon feedback on global climate *Environ. Res. Lett.* **9** 085003

Schaefer K, Zhang T, Bruhwiler L and Barrett A P 2011 Amount and timing of permafrost carbon release in response to climate warming *Tellus* B **63** 165–80

Schneck R, Reick C H and Raddatz T 2013 Land contribution to natural CO_2 variability on time scales of centuries *J. Adv. Model. Earth Syst.* **5** 354–65

Schneider von Deimling T, Grosse G, Strauss J, Schirrmeister L, Morgenstern A, Schhoff S, Meinshausen M and Boike J 2015 Observation-based modelling of permafrost carbon fluxes with accounting for deep carbon deposits and thermokarst activity *Biogeosciences* **12** 3469–88

Schneider von Deimling T, Meinshausen M, Levermann A, Huber V, Frieler K, Lawrence D M and Brovkin V 2012 Estimating the near-surface permafrost-carbon feedback on global warming *Biogeosciences* **9** 649–65

Schuur E A G *et al* 2015 Climate change and the permafrost carbon feedback *Nature* **520** 171–9

Tuomi M, Laiho R, Repo A and Liski J 2011 Wood decomposition model for boreal forests *Ecol. Modelling* **222** 709–18
Tuomi M, Thum T, Järvinen H, Fronzek S, Berg B, Harmon M, Trofymow J, Sevanto S and Liski J 2009 Leaf litter decomposition—estimates of global variability based on yasso07 model *Ecol. Modelling* **220** 3362–71
Tuomi M, Vanhala P, Karhu K, Fritze H and Liski J 2008 Heterotrophic soil respiration—comparison of different models describing its temperature dependence *Ecol. Modelling* **211** 182–90
Zickfeld K, Arora V K and Gillett N P 2012 Is the climate response to CO_2 emissions path dependent? *Geophys. Res. Lett.* **39** L05703